Inorg. Chem. **2003**, *42*, 3026–3035

One-Dimensional Collective Electronic Effects in the Helically Stacked $Cs_2[Ni(CN)_4]\cdot H_2O$ and $Cs_2[Pt(CN)_4]\cdot H_2O$: X-ray Structure, Polarized Specular Reflectance, and ZINDO Calculations

Jeffrey B. Cornelius and Robert M. Trapp

Department of Chemistry, Principia College, Elsah, Illinois 62028

Terry J. Delord, Frank R. Fronczek, and Steven F. Watkins*

Department of Chemistry, Louisiana State University, Baton Rouge, Louisiana 70803

Jill Jasin Orosz and Ronald L. Musselman*

Department of Chemistry, Franklin and Marshall College, Lancaster, Pennsylvania 17604

Received October 10, 2002

The X-ray structure of $Cs_2[Ni(CN)_4]\cdot H_2O$ and the polarized single-crystal UV absorbance spectra of $Cs_2[Ni(CN)_4]\cdot H_2O$ and $Cs_2[Pt(CN)_4]\cdot H_2O$ are presented. The two complexes are isostructural, with helical arrangements of $M(CN)_4^{2-}$ ions in which there is moderate metal–metal electronic perturbation resulting in a spectral red shift from solution in the UV absorbance spectra. In addition, we have modeled the nickel system with a ZINDO calculation of a three-molecule segment of the helix and have found remarkably good agreement with experiment, including excellent reproduction of the red shift. Crystal data are as follows: $Cs_2[Ni(CN)_4]\cdot H_2O$, hexagonal, space group $P6_1$, a = 9.5260(10) Å, c = 19.043(2) Å, V = 1496.5(3) Å^3, T = 100 K, Z = 6, 4335 observed data, R = 0.016, R_w = 0.034.

Introduction

Square planar tetracyano complexes of platinum metals have long been studied for their interesting electronic perturbation along the stacking axis.[1−13] In most cases, this leads to a "solid state effect" which causes the out-of-plane-polarized a_{1g} (d_{z^2}) → a_{2u} (p_z, π^*) transition to red shift and intensify as the planes stack closer.[10,13−16] In extreme cases, such as with partially oxidized $Pt(CN)_4^{2.3+}$ where the stacking is extremely close (~2.9 Å), the stack exhibits metallic reflection and moderate electrical conductivity in the stacking direction.[9,17,18] Our principal interest has been to identify the mechanism of spectral perturbation and its relationship to

* Authors to whom correspondence should be addressed. E-mail: ronald.musselman@fandm.edu (R.L.M.); swatkins@lsu.edu (S.F.W.).

(1) *Extended Interactions between Metal Ions in Transition Metal Complexes*; Interrante, L. V., Ed.; ACS Symposim Series 5; American Chemical Society: Washington, DC, 1974.
(2) *Low-Dimensional Cooperative Phenomena. The Possibility of High-Temperature Superconductivity*; Keller, H. J., Ed.; Plenum: New York, 1975.
(3) *Chemistry and Physics of One-Dimensional Metals*; Keller, H. J., Ed.; Plenum: New York, 1977.
(4) *Synthesis and Properties of Low-Dimensional Materials*; Miller, J. S., Epstein, A. J., Eds.; Annals of the New York Academy of Sciences 313; New York, 1978.
(5) *Highly Conducting One-Dimensional Solids*; Devreese, J. T., Evrard, R. P., van Doren, V. E., Eds.; Plenum: New York, 1979.
(6) *Extended Linear Chain Compounds*; Miller, J. S., Ed.; Plenum: New York, 1981 and 1983.
(7) *Inorganic Compounds with Unusual Properties*; King, R. B., Ed.; ACS Advances in Chemistry Series 150; American Chemical Society: Washington, DC, 1976.
(8) *Inorganic Compounds with Unusual Properties-II*; King, R. B., Ed.; ACS Advances in Chemistry Series 173; American Chemical Society: Washington, DC, 1979.
(9) Musselman, R. L.; Williams, J. W. *J. Chem. Soc., Chem. Commun.* **1977**, 186.
(10) Anex, B. G.; Musselman, R. L. *J. Phys. Chem.* **1980**, *84*, 883.
(11) Musselman, R. L.; Stecher, L. C.; Watkins, S. F. *Inorg. Chem.* **1980**, *19*, 3400.
(12) Musselman, R. L.; Wolfe, B. M.; Brener, N. E.; Gale, R. J.; Goodrich, R. G.; Watkins, S. F. *Solid State Commun.* **1987**, *63*, 595.
(13) Musselman, R. L.; Anex, B. G. *J. Phys. Chem.* **1987**, *91*, 4460.
(14) Moreau-Colin, M. L. *Struct. Bonding (Berlin)* **1972**, *10*, 167.
(15) Yersin, H.; Gliemann, G. *Z. Naturforsch., B: Chem. Sci.* **1975**, *30*, 183.
(16) Lechner, A.; Gliemann, G. *J. Am. Chem. Soc.* **1989**, *111*, 7469.
(17) Williams, J. M.; Schultz, A. J. In *Molecular Metals*; Hatfield, W. E., Ed.; Plenum: NewYork, 1978; p 337.
(18) Gliemann, G.; Yersin, H. *Struct. Bonding (Berlin)* **1985**, *62*, 87.

10.1021/ic026101a CCC: $25.00
Published on Web 03/29/2003

metallic conductivity. The perturbation has been described by some as band formation[19] while others have suggested exciton formation.[20] Interest continues in stacked planes of $Pt(CN)_4^{2-}$ having axial spectral perturbation.[21−23] Both tetracyanoplatinates and -nickelates serve as simple models for more complex systems such as substituted phthalocyanines which are used in photovoltaic devices[24] and as tumor imaging agents.[25]

We previously demonstrated that in stacked planar tetracyanometalates there is an extended perturbation of some sort, extending over at least 20 metal centers using mixed metal stacks of $M(CN)_4^{2-}$ in crystals prepared from mixtures of $Ba[Ni(CN)_4]\cdot 4H_2O$ and $Ba[Pt(CN)_4]\cdot 4H_2O$ with from 5% to 95% $Ba[Pt(CN)_4]\cdot 4H_2O$.[10] At all concentrations, a single out-of-plane-polarized a_{1g} (d_{z^2}) → a_{2u} (p_z, π^*) transition was found whose intensity and energy were proportional to composition as % Pt. In that case, the molecular planes were aligned perpendicular to the stacking direction, and the polarization of the *z*-allowed transition was along the stacking direction.

$Cs_2[Pt(CN)_4]\cdot 4H_2O$ (**1**) has planes that are arranged helically around the *c* axis direction and with a moderate tilt from the helix axis.[26,27] The dihedral angle between adjacent planes is reported as 13.0°,[26] and the angle between plane normals and the *c* axis calculates to be 11.6°. This arrangement separates the bulk "stacking direction" from the molecular out of plane direction and allows for the investigation of whether the polarization direction for the red-shifted a_{1g} (d_{z^2}) → a_{2u} (p_z, π^*) transition is perpendicular to the individual planes or parallel to some collective stacking direction. We report on our polarized specular reflectance spectral study of $Cs_2[Pt(CN)_4]\cdot 4H_2O$.

Since tetracyanonickelates are typically closely isostructural with their platinum counterparts, and we have had prior interest in such nickel complexes,[11,28,29] we ran a parallel study of $Cs_2[Ni(CN)_4]\cdot H_2O$ (**2**). This complex, however, had been structurally studied only with powder diffraction,[27,30] so a single-crystal X-ray diffraction study of $Cs_2[Ni(CN)_4]\cdot H_2O$ was performed. We also report on a polarized specular reflectance spectral study of $Cs_2[Ni(CN)_4]\cdot H_2O$. In addition, we performed a model calculation on a segment of $Cs_2[Ni(CN)_4]\cdot H_2O$ using the semiempirical method, ZINDO, developed by Zerner and others.[31] Our calculation benefited from our recent ZINDO calculation on single-molecule ions of $Ni(CN)_4^{2-}$.[32]

Table 1. Elemental Analyses

	$Cs_2[Ni(CN)_4]\cdot H_2O$		$Cs_2[Pt(CN)_4]\cdot H_2O$	
	theoretical,%	found,%	theoretical,%	found,%
Cs	59.52	59.1	45.6	37.80
Ba	0.00	<0.05	0.00	<0.05
Ni or Pt	13.15	13.37	33.46	31.98
C	10.76	10.76	8.2	5.97
N	12.54	12.49	9.61	9.07
O	3.58	3.45	2.78	
H	0.45	0.46	0.35	0.35

Past spectral assignments of solid-state spectra have been reported using single-molecule symmetry and terminology. The unit cells in these complexes do not retain the molecular symmetry as do many of the straight-stacked salts, and thus we will not be able to use the single-molecule terminology for transitions. Furthermore, as we have shown in our recent paper on the calculation of transitions in the single molecule of $Ni(CN)_4^{2-}$,[32] we will need to expand the traditional concept of state transition to include several orbital transitions in order to fully characterize each transition in these complexes.

Experimental Section

Preparation of $Cs_2[M(CN)_4]\cdot H_2O$. Aqueous solutions of $Cs_2[Ni(CN)_4]$ and $Cs_2[Pt(CN)_4]$ were prepared by the stoichiometric addition of saturated Cs_2SO_4 to $Ba[M(CN)_4]\cdot 4H_2O$ dissolved in a minimum of water. The resulting $BaSO_4$ was filtered out, and the filtrate was slowly evaporated at room temperature for over one week. $Ba[Ni(CN)_4]\cdot 4H_2O$ was prepared as previously described,[28] and $Ba[Pt(CN)_4]\cdot 4H_2O$ was obtained commercially. Elemental analyses are listed in Table 1. While many of the values for the $Cs_2[Pt(CN)_4]\cdot H_2O$ are low and may be due to impurities from starting materials, a Weissenberg X-ray photo of the crystal used for spectroscopy showed agreement with literature values.[26,30,33]

X-ray Data Collection. A golden yellow prismatic crystal of $Cs_2[Ni(CN)_4]\cdot H_2O$ having approximate dimensions 0.12 × 0.15 × 0.16 mm^3 was used for data collection using graphite-monochromated Mo Kα radiation ($\lambda = 0.71073$ Å) on a Nonius KappaCCD diffractometer fitted with an Oxford Cryostream cooler.

Systematic absences 00*l* with $l \neq 6n$ indicated a hexagonal space group $P6_1$ (No. 169) or its enantiomeric group $P6_5$. The former was demonstrated to be the appropriate choice as described in a following paragraph. The data were collected within the range $2.5° < \theta < 35°$ at a temperature of 100 ± 1° K. A total of 27168 reflections, including a complete set of Friedel pairs, was collected: *h* from −15 to 15, *k* from −13 to 13, *l* from −30 to 30.

Data reduction included absorption corrections by the multiscan method, and transmission coefficients ranged from 0.298 to 0.336. A secondary extinction correction was applied.[34] The final coefficient, refined in least-squares, was $2.50(7) \times 10^{-3}$. Redundant

(19) Whangbo, M. H.; Hoffman, R. *J. Am. Chem. Soc.* **1978**, *100*, 6093.
(20) Day, P. *J. Am. Chem. Soc.* **1975**, *97*, 1588.
(21) Brozik, J. A.; Scott, B. L.; Swanson, B. I. *J. Phys. Chem. B* **1999**, *103*, 10566.
(22) Pana, O.; Giurgiu, L. V.; Knorr, S.; Rahmer, J.; Grupp, A.; Mehring, M. *Solid State Commun.* **2001**, *119*, 553.
(23) Brozik, J. A.; Scott, B. L.; Swanson, B. I. *Inorg. Chim. Acta* **1999**, *294*, 275.
(24) McHale, G.; Newton, M. I.; Hooper, P. D.; Willis, M. R. *Opt. Mater.* **1996**, 89.
(25) Mang, T. S.; McGinnis, C.; Liebow, C.; Nseyo, U. O.; Crean, D. H.; Dougherty, T. J. *Cancer* **1993**, *71*, 269.
(26) Johnson, P. L.; Koch, T. R.; Williams, J. M. *Acta Crystallogr., Sect. B* **1977**, *33*, 1293.
(27) Holzapfel, W.; Otto, H. H.; Yersin, H.; Gliemann, G. *J. Appl. Crystallogr.* **1979**, *12*, 241.
(28) Musselman, R. L.; Cornelius, J. B.; Trapp, R. M. *Inorg. Chem.* **1981**, *20*, 1931.
(29) Arndt, G. A.; Danielson, E. D.; Fanta, A. D.; Musselman, R. L. *Inorg. Chem.* **1988**, *27*, 1400.
(30) Otto, H. H.; Holzapfel, W.; Yersin, H.; Gliemann, G. *Z. Naturforsch., B: Chem. Sci.* **1976**, *31*, 528.
(31) Ridley, J.; Zerner, M. *Theor. Chim. Acta* **1973**, *32*, 111.
(32) Mantz, Y. A.; Musselman, R. L. *Inorg. Chem.* **2002**, *41*, 5770.
(33) The values measured from a 0-level Weissenberg photograph were the following: $\beta = 120.1(2)°$, $a = 9.65(3)$ Å, $b = 9.71(3)$ Å. Literature values include the following: $\beta = 120.0°$, $a = b = 9.709(4)$ Å (ref 26) and 9.687(2) Å (ref 30).
(34) Zachariasen, W. H. *Acta Crystallogr.* **1963**, *16*, 1139.

Table 2. Selected Crystallographic Parameters

formula	$Cs_2[Ni(CN)_4]\cdot H_2O$
M_r	446.63
space group	hexagonal; $P6_1$
a	9.5260(10) Å
c	19.043(2) Å
V	1496.5(3) Å^3
Z	6
radiation	Mo Kα, $\lambda = 0.71073$ Å
T	100 K
indep reflns	4396
R_{int}	0.040
θ_{max}	35.0°
R [$F^2 > 2\sigma(F^2)$]	0.016
R_w (F^2)	0.034

data were averaged, $R_{int} = 0.040$, yielding 4396 unique data, of which 4335 had $I > 2\sigma(I)$. (We also ran a room temperature study of this compound and found the lattice constants to be $a = 9.554(1)$ Å and $c = 19.292(3)$ Å.)

Structure Solution and Refinement. The structure was solved using heavy-atom methods. The hydrogen atoms of the water molecule were located from a difference map and were refined isotropically, with U_{iso} values assigned as $1.5U_{eq}$ of the oxygen atom.

Scattering factors were taken from Cromer and Waber.[35] Anomalous dispersion effects were included in F_c;[36] the values for $\Delta f'$ and $\Delta f''$ were those of Cromer.[35] Refinement of 116 parameters using SHELXL[37] converged in $P6_1$ with $R = 0.016$ and $R_w = 0.034$. Refinement of the Flack parameter[38] yielded a value of 0.017(17); thus, $P6_1$ was proven correct. The highest peak in the final difference Fourier was 0.61 e/Å^3; the minimum negative peak was -0.44 e/Å^3. Selected experimental crystallographic values are given in Table 2.

Spectral Measurements. Due to the high spectral extinction coefficients for this system, room-temperature polarized spectra were obtained through specular reflectance rather than transmission. The reflectance instrument, based on a concept by Anex,[39] was essentially a grating microspectrophotometer consisting of tungsten-halogen and xenon arc light sources, an Instruments SA HR320 0.32 m computer controllable grating monochromator, a Glan-Thompson polarizer, a double-beam reflecting microscope, and a photomultiplier detector. Signal detection was through two Princeton Applied Research 186A lock-in amplifiers, and instrument control resided on an Apple IIe computer. The data were uploaded to a Hewlett-Packard 3000 computer for processing. Reflectance was measured relative to a NIST standard second-surface mirror. Kramers−Kronig transformation of the reflectance data provided standard absorbance values. Since Kramers−Kronig transformation requires reflectance data over energies from 0 to ∞, an effective transition was added at energies higher than the experimental region and adjusted so that the valleys in the transformed data resembled those from solution data. We assumed that the infrared reflectance was constant and at the level of the lowest-energy measured reflectances for both compounds. The effective transitions in the far UV are summarized in the Supporting Information (SI), Table S-1; they had no effect on energies of transitions but did affect intensities. Polarized single-crystal specular reflectance spectra were taken on natural faces with the electric vectors parallel to and perpendicular to the needle (c) direction, which was coincident with the helix axis.

Solution spectra were obtained on a Perkin-Elmer Lambda 40 UV−vis spectrophotometer at room temperature.

Semiempirical Calculations. Both ground-state energies and allowed electronic transitions for $Cs_2[Ni(CN)_4]\cdot H_2O$ were calculated using the Zerner-modified semiempirical INDO (intermediate neglect of differential overlap) method known as ZINDO.[31] The version of ZINDO we use here is contained in the CAChe suite of programs from Fujitsu.[40] It had been extremely successful in calculating theoretical electronic spectra of the dianion, $Ni(CN)_4^{2-}$.[32] The experimental and calculated transitions for the two lowest-energy charge transfer transitions matched remarkably well in both energy and intensity. In addition, the lowest-energy x,y-polarized transition ($A_{1g} \rightarrow E_u$) required several orbital transitions to be accurately characterized. The concept of linear combinations of orbital transitions was discussed and has been utilized in the present study as well.

Because the ZINDO technique is semiempirical, the calculation parameters typically need to be optimized in order for the calculated electronic spectrum to match the experimental spectrum as closely as possible. The CAChe implementation of ZINDO includes default values for numerous parameters.[32] The parameters most commonly adjusted in transition metal complexes are the resonance integrals for the central metal, β_s, β_p, and β_d.[41] β_s and β_p are set equal ("β_{sp}") and represent the amount of interaction between s and p orbitals on the metal and those on adjacent ligand atoms. The β_d values represent interaction of the metal d orbitals with ligands. Values which are more negative represent a greater interaction between the corresponding metal orbital(s) and the ligand orbitals. We used the optimized β parameters from our recent work[32] as parameters in this current work: $\beta_{sp} = -5$ and $\beta_d = -41$. In determining transition energies, ZINDO uses a process known as configuration interaction (CI). The CI process in ZINDO considers the effects of single-electron excitations from a set of filled orbitals to a set of virtual orbitals. The "CI level" is an integer representing the number of orbitals in each region used in the CI calculation. Since the ZINDO CI in CAChe is singly excited, the choice of CI level in this case affects only the state transitions and not the individual orbital energies or wave functions.[32] We found that a CI level of 10 was the maximum suitable for all transitions but that the z-polarized transitions could be accurately modeled with a CI level of 6.

Calculations were carried out on only $Cs_2[Ni(CN)_4]\cdot H_2O$ since ZINDO parameters are not reliable for the platinum case; spin−orbit coupling which is expected to be significant in a platinum complex is not accounted for by ZINDO, and we felt that assignment of the $Cs_2[Pt(CN)_4]$ spectra could reasonably be compared to those for $Cs_2[Ni(CN)_4]$. Previous work of ours has found spectral similarity in the two systems.[10]

Results

Description of the Structure. The crystal structure of $Cs_2[Ni(CN)_4]\cdot H_2O$ consists of hexagonal unit cells containing six formula units. Tetracyanonickelate dianions are stacked in spirals around the crystallographic 6-fold screw axes, Figure 1, with cesium cations and water molecules wound around the periphery of the spirals.

$Ni(CN)_4^{2-}$. The anion deviates slightly but significantly from planarity. Opposite N atoms N1 and N2 lie, respec-

(35) Cromer, D. T.; Waber, J. T. *International Tables for X-ray Crystallography*; The Kynoch Press: Birmingham, England, 1974.
(36) Ibers, J. A. *Acta Crystallogr.* **1964**, *17*, 781.
(37) Sheldrick, G. M. *SHELXL97*; University of Göttingen: Göttingen, Germany, 1997.
(38) Flack, H. D. *Acta Crystallogr.* **1983**, *A39*, 876.
(39) Anex, B. G. *Mol. Cryst.* **1966**, *1*, 1.
(40) Zerner, M. C. *ZINDO (in CAChe)*; Fujitsu Limited: Beaverton, OR, 2000.
(41) Anderson, W. P.; Edwards, W. D.; Zerner, M. C. *Inorg. Chem.* **1986**, *25*, 2728.

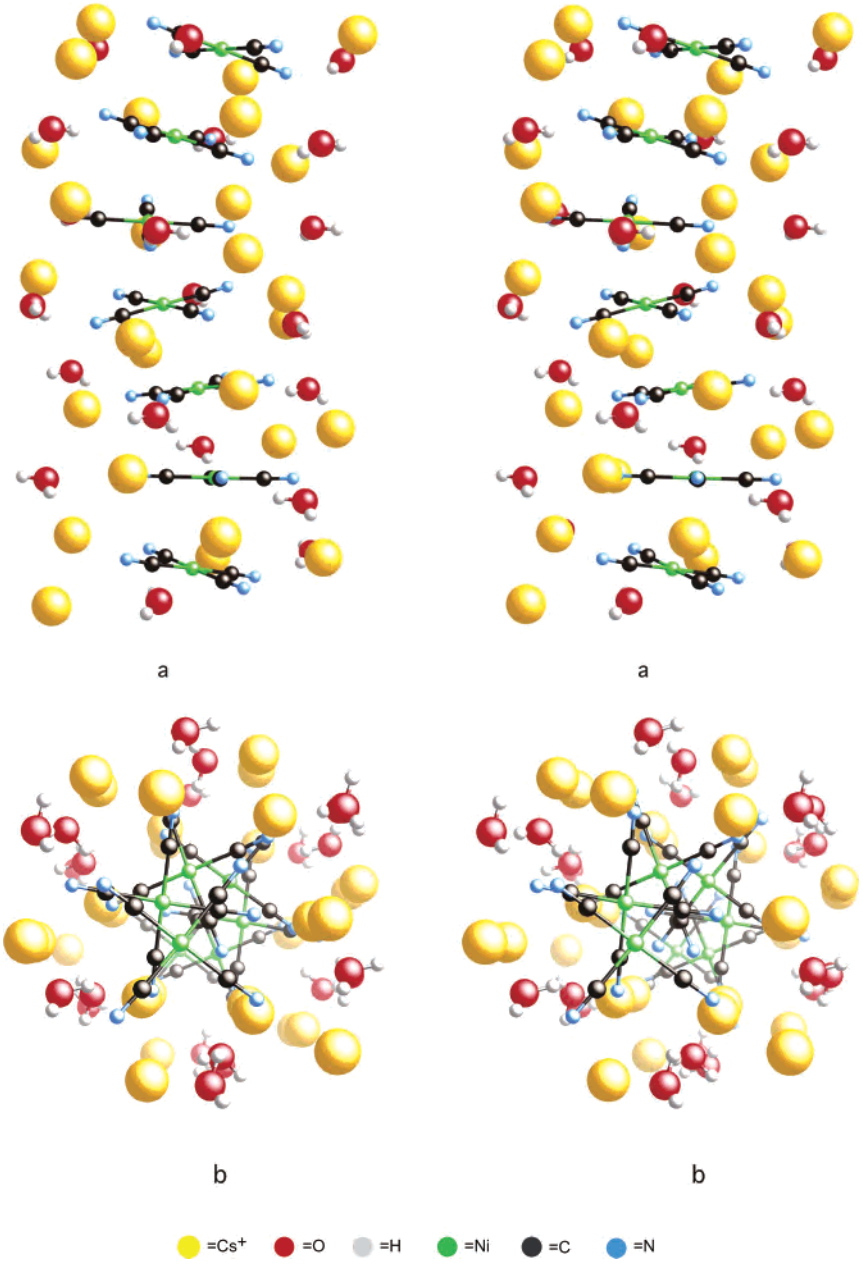

Figure 1. Stereoviews of a single helical chain of $Ni(CN)_4^{2-}$ ions with associated Cs^+ ions and water molecules: (a) side view, (b) top view.

tively, 0.023(2) and 0.016(2) Å on the same side, out of the best plane of the other seven atoms, which exhibit a mean deviation of 0.004 Å. The mean Ni−C and C−N bonds are 1.868 and 1.157 Å, respectively, comparable to previous observations.[42] Each anion is tilted 12.7(1)° from the *c*-axis, and 12.61(5)° with respect to adjacent anions in the spiral. The distance between adjacent Ni centers in the spiral is 3.507(1) Å, with a Ni···Ni···Ni angle of 155.4(1)°. At 298 K, the Ni···Ni distance is longer (3.556(2) Å) as a result of the 1.3% expansion of the length of the *c* axis from 100 to 298 K.

Cs^+. The coordination number of each cesium is eight, but the two coordination polyhedra are not the same. The Cs1 coordination polyhedron (Figure S2) is a distorted square antiprism, while the Cs2 coordination polyhedron (Figure S3) is best described as a distorted bicapped trigonal prism. These two polyhedra share a square face composed of the tightly bound water molecule and three N atoms from anions in two adjacent spirals (Figure S4). Thus, the cesium ions are paired.

H_2O. The water molecule is bound tightly to two cesium ions (O···Cs1 = 3.079(2) Å, O···Cs2 = 3.114(2) Å) and, through H-bonding, to nitrogen atoms in two adjacent spirals. One of the H-bonds is strong (O1···N3 = 2.812(3) Å, O1−H···N3 = 173(4)°), while the other is weaker (O1···N4 = 3.065(3) Å, O1−H···N4 = 165(3)°). The arrangement is tetrahedral. A longer contact with another Cs1 atom (3.516(2) Å) completes the coordination polyhedron of the water molecule. In the unit cell, the water molecules occupy two discrete channels along the crystallographic

(42) Larsen, F. K.; Hazell, R. G.; Rasmussen, S. E. *Acta Chem. Scand.* **1969**, *23*, 61.

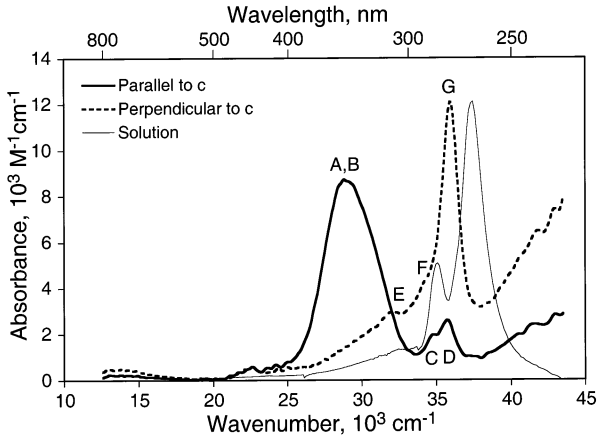

Figure 2. Transformed absorbance spectra of $Cs_2[Ni(CN)_4]\cdot H_2O$, shown with a solution spectrum of $Ni(CN)_4^{2-}$, illustrating a red shift upon crystallization.

Table 3: Selected Bond Lengths (Å) and Angles (deg)

Ni		C1	1.874(2)	N1		C1	1.156(3)
Ni		C2	1.879(2)	N2		C2	1.159(3)
Ni		C3	1.855(2)	N3		C3	1.153(3)
Ni		C4	1.865(2)	N4		C4	1.160(3)
C1	Ni	C2	177.96(9)	C3	Ni	C4	179.71(11)
C1	Ni	C3	90.32(9)	Ni	C1	N1	179.1(2)
C1	Ni	C4	89.49(10)	Ni	C2	N2	177.1(2)
C2	Ni	C3	87.70(9)	Ni	C3	N3	179.0(2)
C2	Ni	C4	92.49(10)	Ni	C4	N4	179.1(2)

3-fold screw axes. Selected bond lengths and angles are in Table 3. Complete crystallographic data may be found in Table S2.

Spectroscopic Results. The polarized specular reflectance spectra of $Cs_2[Ni(CN)_4]\cdot H_2O$ are shown in the Supporting Information (SI), Figure S5, and those of $Cs_2[Pt(CN)_4]\cdot H_2O$ are shown in Figure S6. Prominent maxima in the reflectance spectra are indicative of strong absorbances but are not directly useful for comparison with energies of absorption spectra or for intensities. Maxima in specular reflectance spectra fall at slightly lower energies than the corresponding absorbance peaks.

$Cs_2[Ni(CN)_4]\cdot H_2O$. Figure 2 shows the Kramers−Kronig transformed absorbance data for two polarizations on a side face (100) of $Cs_2[Ni(CN)_4]\cdot H_2O$: with the electric vector aligned parallel and perpendicular to the *c* (helical) axis. Included is a solution spectrum of $K_2[Ni(CN)_4]$. The solution was sufficiently dilute (6×10^{-5} M) to avoid spectral perturbations due to oligimers.[16] The two prominent features of the crystalline material are a relatively low energy peak in the parallel spectrum at 29.3 kcm^{-1} and a sharp peak at 35.8 kcm^{-1} in the perpendicular spectrum. Both of these peaks appear to have been significantly red-shifted and increased in intensity from corresponding solution peaks at 34.9 and 37.2 kcm^{-1} which have been demonstrated to be *z*- and *x*,*y*-polarized, respectively.[11] Similar solid-state peaks have appeared in earlier tetracyanometalate spectra,[10,28] most prominently in $Ba[Ni(CN)_4]\cdot 4H_2O$.[10] The lowest energy peak at 29.3 kcm^{-1} is reminiscent of the red-shifted out-of-plane-polarized "solid state" band in $Ba[Ni(CN)_4]\cdot 4H_2O$ and other salts with stacked planes which have been assigned as $A_{1g} \rightarrow A_{2u}$ (a_{1g} (d_{z^2}) → a_{2u} (p_z, π^*)).[10,28] This transition appears at various energies dependent on the stacking distance between $Ni(CN)_4^{2-}$ planes. In order to relate this peak in $Cs_2[Ni(CN)_4]\cdot H_2O$ to that in other $Ni(CN)_4^{2-}$ salts, we have shown the energy of this transition as a function of stacking distance for two other $Ni(CN)_4^{2-}$ salts[10,28] in Figure 3. The least-squares line falls close to all three data points, suggesting that the 29.3 kcm^{-1} peak in $Cs_2[Ni(CN)_4]\cdot H_2O$ is analogous to the other two peaks. It is important to note that for the other $Ni(CN)_4^{2-}$ salts this transition is *z*-polarized (out of plane), whereas the orientation of the electric vector in this case is along the helix axis which is about 12.5° from the out of plane direction. We will discuss the consequences of this shortly. The other prominent transition in Figure 2 appears in the perpendicularly polarized spectrum, at 35.8 kcm^{-1}. This appears to correspond to the solution peak at 37.2 kcm^{-1} and also to the lowest energy in-plane transition in $Ba[Ni(CN)_4]$ which has been assigned as $A_{1g} \rightarrow E_u$ (e_g (d_{xz}, d_{yz}) → a_{2u} (p_z, π^*)).[28]

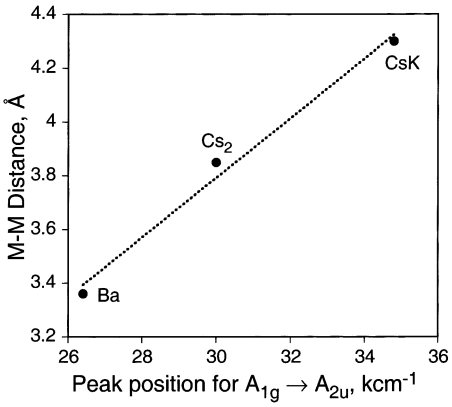

Figure 3. Metal−metal distance vs peak position for the lowest-energy transition related to the $A_{1g} \rightarrow A_{2u}$ single molecule transition in three $Ni(CN)_4^{2-}$ salts.

Further examination of Figure 2 shows that there is a significant peak in the parallel-to-*c*-polarized spectrum underneath the prominent 35.8 kcm^{-1} perpendicular spectrum. Since the $Ni(CN)_4^{2-}$ planes have a 12.58° tilt with respect to the needle, or helix, axis which is also the orientation of the electric vector, one expects to see such an "in-plane" component in a parallel-polarized spectrum. By the same argument, however, if the transitions indeed involved molecular orbitals confined to a single planar complex ion, one would also expect some "out-of-plane" component to appear in the perpendicular spectrum under the prominent 29.3 kcm^{-1} peak. No component is seen in this region, however. We will wait until after the results from our ZINDO calculations have been presented to revisit this apparent discrepancy. Note also that there is a significant hump at about 32 kcm^{-1}; this has no obvious equivalent in the previously reported spectra.[10,11,28]

$Cs_2[Pt(CN)_4]\cdot H_2O$. Figure 4 shows both polarizations of the spectrum for $Cs_2[Pt(CN)_4]\cdot H_2O$ after Kramers−Kronig transformation to absorbance values along with a solution spectrum of $Ba[Pt(CN)_4]\ ]\cdot 4H_2O$. The most notable difference from solution to solid state is the very intense peak A at 28.6 kcm^{-1}. The relatively small peak in the solution

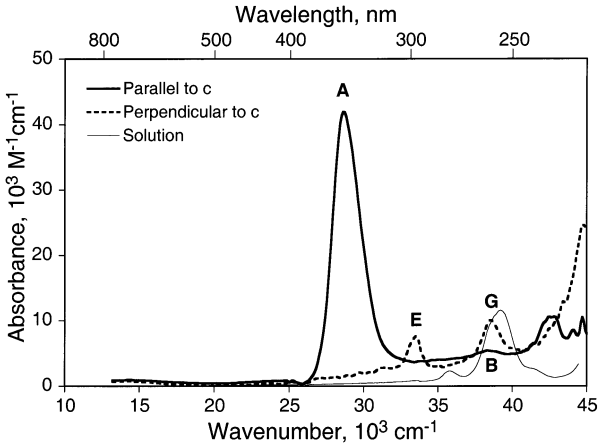

Figure 4. Transformed absorbance spectra of $Cs_2[Pt(CN)_4]\cdot H_2O$ shown with a solution spectrum of $Pt(CN)_4^{2-}$, illustrating a large red shift and intensity increase of peak A upon crystallization.

spectrum at 35.7 kcm^{-1} appears to be the origin of peak A by analogy with the $Ni(CN)_4^{2-}$ case and a similar analogy with the *z*-polarized transition in $Ba[Pd(CN)_4]\cdot 4H_2O$.[13] Peak A in this platinum complex differs from the parallel-to-*c*-polarized transition in $Cs_2[Ni(CN)_4]\cdot H_2O$ at 29 kcm^{-1} with its much higher intensity: $\epsilon_{max} = 42\,000\ M^{-1}\ cm^{-1}$ compared with 9000 $M^{-1}\ cm^{-1}$ for the nickel complex. Peak G appears to be derived from the solution peak at 39.1 kcm^{-1}. The region around 38−39 kcm^{-1} is quite similar to that for the 35 kcm^{-1} region in $Cs_2[Ni(CN)_4]\cdot H_2O$, including the peak intensities and the residual intensity in the parallel spectrum beneath the prominent peak in the perpendicular spectrum. Also, peak E at about 34 kcm^{-1} seems to be a larger version of the as-yet-unexplained bump in the $Cs_2[Ni(CN)_4]\cdot H_2O$ spectrum at 32 kcm^{-1}. While the transitions will prove to be similar to those in the nickel complex, we will wait until our calculations have been presented to provide assignments to these transitions.

ZINDO Calculation Results. Our objectives in performing ZINDO calculations on $Cs_2[Ni(CN)_4]\cdot H_2O$ were to model as well as possible with a relatively easy-to-use routine the transition energies of the solid-state system and thus have a result to aid in the assignment of transitions. Our work on a single $Ni(CN)_4^{2-}$ dianion[32] was focused on selecting parameters that would result in calculated spectra that most closely resembled experimental spectra; a singly excited CI level of 10 was found to be best for all transitions, but the *z*-polarized transition could be accurately modeled with CI = 6. The maximum CI level available with the CAChe suite of programs is 22. While it would be most desirable to model an extended helical chain of $Ni(CN)_4^{2-}$ complex ions, practical limitations dictated a set of three planes in the helix. Since the CI level for a set of three planes would be expected to be three times that required for single plane, the limit of CI = 22 would be satisfactory for the *z*-polarized transition(s). The *x*,*y*-polarized transitions, however, may be underprocessed for configuration interaction with three planes and CI = 22, but from our earlier work, we showed that a CI level in the range of 7 gave a reasonable approximation to experiment, although not the remarkably close agreement from the CI = 10 calculation. We felt that using CAChe with a CI level of 22 on three planes would hopefully give a reasonable suggestion of the solid-state electronic environment. Agreement with experiment would, of course, be a clear test of the reasonableness of the model and method, but even a partial reproduction of the red shift that occurs in the solid state for both *x*,*y*- and *z*-polarized transitions would be especially rewarding, particularly in light of the extremely limited (three-plane) model chosen.

The objective of our calculations in this report is to identify the orbital involvement and if possible the transition polarizations of the experimental transitions in the three regions of interest. This means that we will emphasize state transition

Table 4. Experimental and Calculated Spectral Parameters

exptl (Gaussian deconvolution)			calcd								
				transition moment							
curve	peak energy, k cm^{-1}	max abs ϵ	state trans	*x*	*y*	*z*	trans energy, k cm^{-1}	osc strength	adj abs $10^3\ M^{-1}\ cm^{1a}$	halfwidth k cm^{-1}	assignment
						Ni Parallel to *c*					
A	28.45	5.23	1 → 5	0.950	−0.186	−3.136	28.130	0.143	4.131	2.5	$9a_{1g} \rightarrow 4a_{2u}{}^c$
B	30.25	4.56	1 → 15	−0.105	0.113	−2.577	32.470	0.102	2.950	2.5	$9a_{1g} \rightarrow 4a_{2u}{}^c$
C	34.70	1.18									
D	35.75	1.62	*b*								$2e_g \rightarrow 4a_{2u}{}^c$
						Ni Perpendicular to *c*					
E	32.10	0.63	1 → 12	0.650	2.166	0.285	31.740	0.078	1.404	2.0	$2e_g \rightarrow 4a_{2u}{}^d$
			1 → 13	2.271	−0.647	0.368	32.200	0.087	1.567	2.0	$2e_g \rightarrow 4a_{2u}{}^d$
	33.90	0.87									
F	34.75	1.73									
G	35.95	8.85	1 → 20	2.428	−0.624	0.224	36.440	0.109	1.967	2.0	$2e_g \rightarrow 4a_{2u}{}^d$
			1 → 21	0.768	1.084	−0.759	36.560	0.040	0.729	2.0	$2e_g \rightarrow 4a_{2u}{}^d$
			1 → 22	1.357	−3.564	0.201	36.670	0.252	4.557	2.0	$2e_g \rightarrow 4a_{2u}{}^d$
			1 → 23	−2.965	−1.828	−0.692	36.730	0.218	3.946	2.0	$2e_g \rightarrow 4a_{2u}{}^d$
						Pt Parallel to *c*					
A	28.60	35.94									$A_{1g} \rightarrow A_{2u}{}^c$
B	38.30	0.82									$A_{1g} \rightarrow A_{2u}{}^c$
						Pt Perpendicular to *c*					
E	33.45	4.73									$A_{1g} \rightarrow E_u{}^c$
G	38.55	5.53									$A_{1g} \rightarrow E_u{}^c$

[a] *c*-Polarized divided by 3; perpendicular to *c* divided by 6. See text. [b] Part of 1 → 22 and 1 → 23 appear in parallel direction. See text. [c] Transition derived from these states. [d] Transition primarily derived from these states.

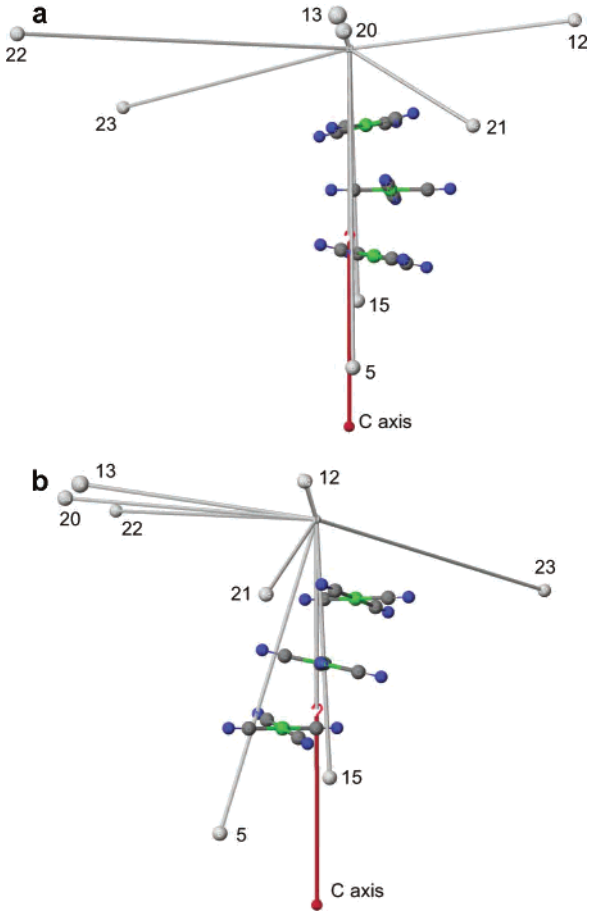

Figure 5. Transition moments for the eight most intense calculated transitions in $Cs_2[Ni(CN)_4]\cdot H_2O$: (a) and (b) two orthogonal views normal to the *c* axis.

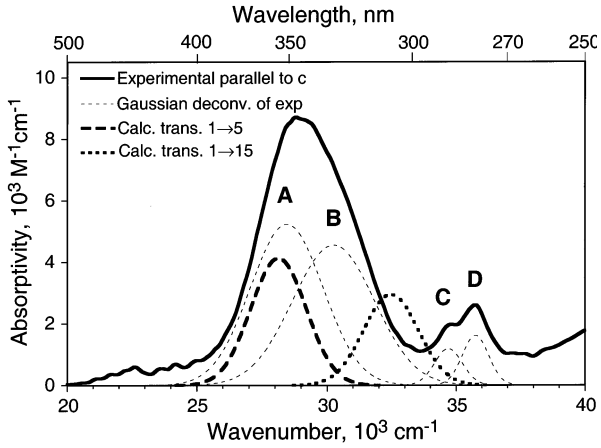

Figure 6. *c*-Polarized experimental and calculated spectra for $Cs_2[Ni(CN)_4]\cdot H_2O$. See text for explanation of transition $1 \rightarrow n$.

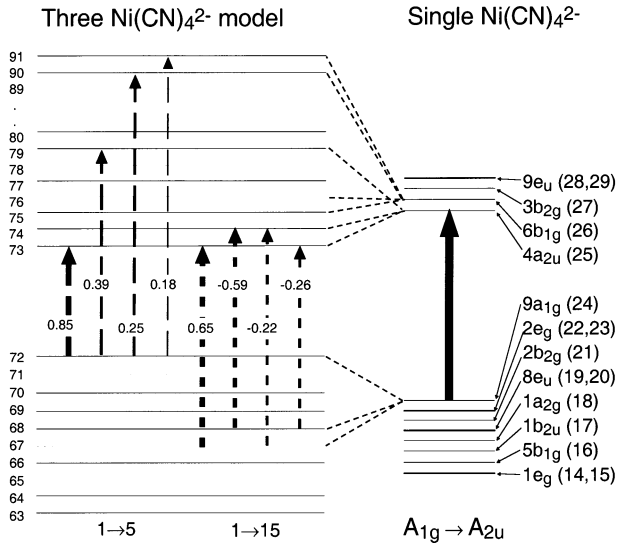

Figure 7. Orbital transition components of the state transitions related to the single-molecule $A_{1g} \rightarrow A_{2u}$ state transition. The coefficients for each orbital transition are overlaid on the transition arrows.

energies, polarizations, orbital transition components, and the wave functions, but it is also interesting to look at the orbital energies resulting from the calculations. In our previous work on a single $Ni(CN)_4^{2-}$ ion, we included only that ion and not any surrounding cations although this would result in an overall negative charge which tends to distort energies somewhat.[43] The energies were in excellent agreement with ab initio calculations.[32] When the ionic charge is increased to −6, however, we have observed that the orbital energies are dramatically elevated (one expects the Fermi level to be close to 0 eV, but instead, it is about 12 eV while the HOMO − 51 level is closest to 0), but as will be seen, the transition energies are in quite good agreement with experiment. We chose to not include counterions for charge neutralization because of the inability to assign noninteger charges in CAChe, and the use of only six whole charges would result in greatly distorted orbital shapes, thereby altering the polarizations of transitions. The energies of the 123 molecular orbitals are listed in the SI, Table S-3. While these are much higher than we expect due to the aforementioned unbalanced charge on the set of three planes, the transition energies depend on relative orbital energies and configuration interaction, and the transition polarizations depend on the MO geometries, both of which we believe are not significantly affected by the charge on the model.

The calculated electronic spectrum for our model of $Cs_2[Ni(CN)_4]\cdot H_2O$ includes numerous absorptions due of course to numerous state transitions. It is important to note, though, that each state transition is in turn composed of several orbital transitions as was the case for one of the transitions in the single-molecule study.[32] We have selected a set of state transitions which have oscillator strengths of at least 0.04 and which are listed in Table 4. A more complete set of state transitions and their component orbital transitions is given in the SI, Table S-4. Since there is no symmetry above C_1 for this segment of three planes, we will simply assign transition designations numerically as they are given in the ZINDO output in CAChe ($1 \rightarrow n$, where 1 refers to the ground state and *n* the excited state). From Table 4, it is evident that there are two transitions, $1 \rightarrow 5$ and $1 \rightarrow 15$, with predominately *c*(*z*) character, where *c* is along the helical axis. This is illustrated graphically in Figure 5 where the spheres marked 5, 15, etc. represent the several transition moment vectors for $1 \rightarrow 5$, $1 \rightarrow 15$, etc. Transition $1 \rightarrow 5$ is

(43) Cory, M. G.; Zerner, M. C. Personal communication.

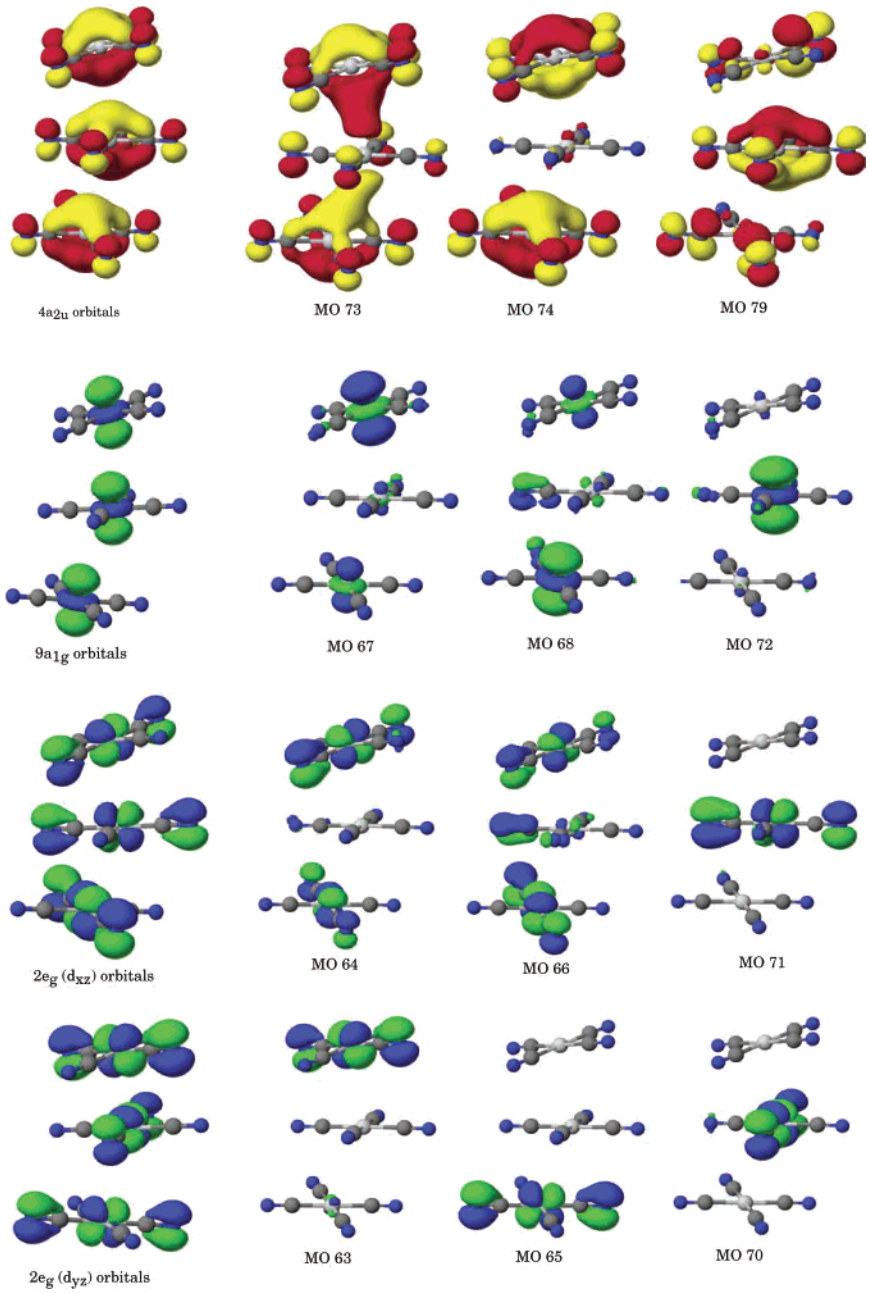

Figure 8. MOs principally involved in transitions of interest, and their uncombined origins on the left.

close to the metal−metal direction, and transition 1 → 15 is close to the helical axis direction; for the purposes of this model, we will assume that they are both generally in the *c* direction. Transitions 1 → 12, 1 → 13, 1 → 20, and 1 → 22 are close to perpendicular to the *c* axis, while transition moments 1 → 21 and 1 → 23 have significant amounts of *c* in them.

The calculated *c*-oriented transitions 1 → 5 and 1 → 15 are depicted along with our experimental *c*-polarized spectrum for $Cs_2[Ni(CN)_4]\cdot H_2O$ in Figure 6. The shapes and energies of the deconvoluted experimental peaks are variable to some extent, of course, but the asymmetry of the experimental peak makes it clear that more than one transition is present. The simple three-plane model shows remarkable agreement with experiment: transition 1 → 5 agrees very closely with peak A, and transition 1 → 15 is reasonably close to peak B. The calculated oscillator strengths have been divided by 3 in order to agree with the absorbance data where the intensities are essentially per molecule. Peaks C and D will be discussed after the remaining calculated transitions have been presented.

In Figure 7, we have shown the four most significant contributors to each of state transitions 1 → 5 and 1 → 15 on a schematic energy-level diagram with their coefficients listed on each arrow. To the right is the one orbital transition comprising the single-molecule $A_{1g} \rightarrow A_{2u}$ state transition, $9a_{1g}$ (d_{z^2}) → $4a_{2u}$ (p_z, π^*).[32] The single-molecule origins of selected MOs in the three-stack model are shown with dashed lines. In Figure 8, the orbitals involved in most of the transition components are illustrated. In the three-molecule model, the three $9a_{1g}$ orbitals from the $Ni(CN)_4^{2-}$ ions have essentially become MOs 67, 68, and 72, and the three $4a_{2u}$

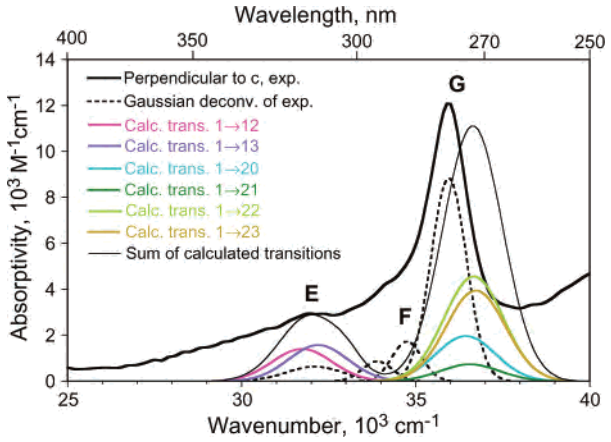

Figure 9. Perpendicular-to-*c* experimental and approximately perpendicular-to-*c* calculated spectra for $Cs_2[Ni(CN)_4]\cdot H_2O$.

orbitals appear primarily in MOs 73, 74, and 79. Note that MO 73 shows extended vertical orbital lobes (tilted because of the helical arrangement of the planes) indicating a significant delocalization of electron density along the metal chain. We earlier proposed such a scenario to explain some of the collective effects we had observed in similar compounds.[10,13] At least 86% of the transition intensity of state transitions 1 → 5 and 1 → 15 are from and to these derivatives of the orbital components of the single molecule $A_{1g} \rightarrow A_{2u}$ transition. Thus, we assign transitions 5 and 15 as correlating with the $A_{1g} \rightarrow A_{2u}$ ($9a_{1g}$ (d_{z^2}) → $4a_{2u}$ (p_z, π^*)) single-molecule state transition.

As was also the case with the single molecule, the perpendicular-to-*c* transitions are much more complex than the parallel transitions. Figure 9 depicts the remaining prominent calculated transitions compared with the experimental perpendicular-to-*c* polarized absorbance spectrum. Two regions of calculated absorbance agree well with the experimental hump E at 32 kcm^{-1} and peak G at about 36 kcm^{-1}. The four largest orbital transition contributors to each of the six state transitions in regions E and G are illustrated in the left $^3/_4$ of Figure 10; in the right $^1/_4$ are the orbital transition components of the single-molecule state transition, $A_{1g} \rightarrow E_u$.[32] In addition, as with the "*z*-polarized" case, the single-molecule origins of selected MOs in the three-stack model are shown with dashed lines. All 24 of the orbital transition components shown are related to one or both of the single-molecule orbitals associated with the $A_{1g} \rightarrow E_u$ single-molecule state transition. In all cases except one (1 → 20, where the value is 43%), at least 74% of the total intensity of each state transition is from orbital transitions related to *both* the origin and target orbitals in the principal orbital transition component ($2e_g$ (d_{xz}, d_{yz}) → $4a_{2u}$ (p_z, π^*)) in the single molecule. This establishes that the intensity in both regions E and G is derived from the $A_{1g} \rightarrow E_u$ single-molecule state transition.

One additional item regarding energies and orbital transition components is of interest. The two transitions in region E have their orbital transition origins in MOs 70 and 71 which, as Figure 8 shows, have their wave functions concentrated on the middle complex plane, whereas those in the higher energy region G have their origins from MOs 63, 64, 65, and 66 which are concentrated on one or both of the outer planes of the set of three. A similar pattern is seen in the *c*-polarized transitions in Figure 7. The lower-energy transition 1 → 5 has all of its orbital component transitions originating on MO 72 which is essentially the inner d_{z^2} orbital, and transition 1 → 15 has its component transitions starting from MOs 67 and 68, consisting of essentially the outer two d_{z^2} orbitals. These observations may relate to evaluating the most accurate infinite-chain modeling configuration. One might propose that orbitals concentrated on the

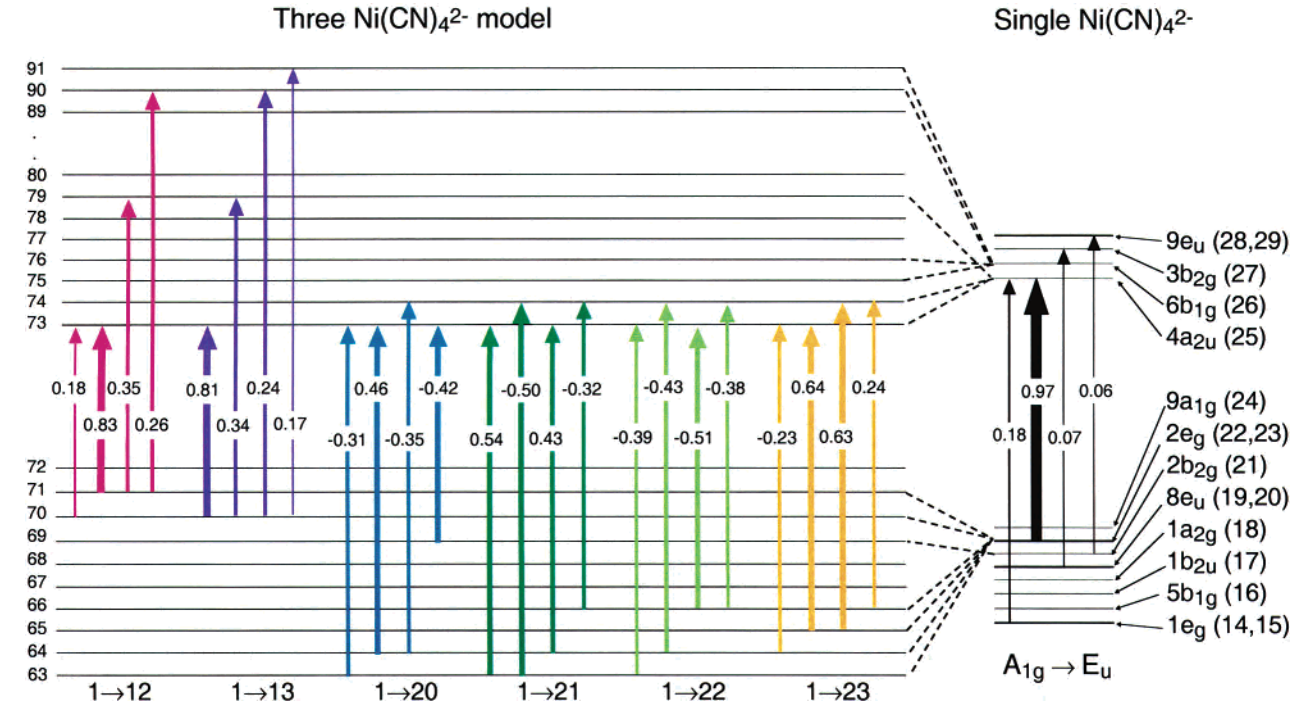

Figure 10. Orbital transition components of the state transitions for a 3-stack of $Cs_2Ni(CN)_4$ related to the single-molecule $A_{1g} \rightarrow E_u$ state transition.

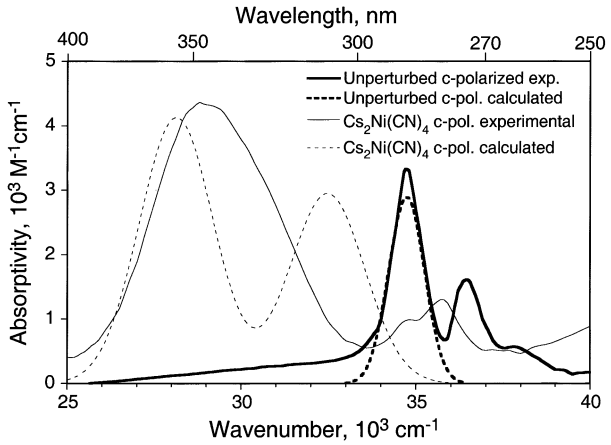

Figure 11. *c*-Polarized experimental and calculated comparisons of perturbed ($Cs_2[Ni(CN)_4]\cdot H_2O$) and unperturbed ($CsK[Ni(CN)_4]$) (refs. 11 and 32) transitions.

inside of the three-plane model have a more realistic environment than those on the outside of the model. This appears to be a reasonable suggestion, especially with regard to the *c*-polarized transitions, where transition $1 \rightarrow 5$ falls very close to experiment while transition $1 \rightarrow 15$ is somewhat to the blue of experiment. The other six transitions all model experiment well, so the distinction for them is somewhat moot.

Discussion

Transition Moments. With the calculation results in hand, we can look at peak D in Figure 6. From Figure 5, it can be seen that two state transitions, $1 \rightarrow 21$ and $1 \rightarrow 23$, have a significant *c*-polarized component. We believe that peak D in the *c*-polarized spectrum is from transitions similar to $1 \rightarrow 21$ and $1 \rightarrow 23$ in the infinite chain which also have a *c*-polarized composition. Peaks C (Figure 6) and F (Figures 6 and 9) which have the same energies and similar intensities have no corresponding transition in our three-molecule model and thus cannot be assigned from our calculated model. Their similarity suggests that they may have the same origin and could possibly be derived from the symmetry-forbidden transition, $A_{1g} \rightarrow B_{1u}$.

Solid-State Effect. Finally, we can look at the spectral perturbation upon crystallization. Figure 11 shows both unperturbed and perturbed spectra. The unperturbed spectra are the *z*-polarized experimental spectrum for $CsK[Ni(CN)_4]$[11] and the ZINDO-calculated *z*-polarized spectrum from our single-molecule paper.[32] The perturbed spectra are the experimental $Cs_2[Ni(CN)_4]\cdot H_2O$ *c*-polarized spectrum and the ZINDO-calculated transitions $1 \rightarrow 5$ and $1 \rightarrow 15$. Both of the latter two spectra show the dramatic red shift upon closer stacking in the crystal (Ni−Ni in $CsK[Ni(CN)_4]$ = 4.20 Å; Ni−Ni in $Cs_2[Ni(CN)_4]\cdot H_2O$ = 3.85 Å) as also illustrated earlier in Figure 4. One of the most satisfying results from our ZINDO calculation is the excellent red shift and intensity increase obtained for transition $1 \rightarrow 5$ at 28 kcm^{-1}. The lesser degree of agreement of transition $1 \rightarrow 15$ at 32.5 kcm^{-1} is understandable in light of the arguments in the previous paragraph, while the integrated intensity has again increased. In both calculated transitions, however, both the red shift and intensity increase are present and suggest that a simple linear combination of molecular orbitals is sufficient to reproduce the solid-state effect in complexes such as this, and thus, this simple model is also a reasonable explanation for the effect experimentally.

$Cs_2[Pt(CN)_4]\cdot H_2O$. In Figure 4, peak A may now be assigned as having derived from the $A_{1g} \rightarrow A_{2u}$ single-molecule transition since it is polarized along the *c* axis and has red-shifted significantly from the unperturbed solution position.[10] Peak G is close to the *x*,*y*-polarized $A_{1g} \rightarrow E_u$ transition in the $Pt(CN)_4^{2-}$ solution spectrum,[29,44] so it is likely derived from that state transition. In addition, the relative intensities and positions of peaks G and D reflect those in the same peaks in $Cs_2[Ni(CN)_4]\cdot H_2O$. We thus assign peak G as due to state transitions polarized close to perpendicular to the *c* axis as well as those with some *c* axis components. All are derived from the $A_{1g} \rightarrow E_u$ transition in the single $Pt(CN)_4^{2-}$ ion. Peak D is from the state transitions appearing in peak G which are polarized partially parallel to *c*. Peak E is cleanly polarized in the perpendicular-to-*c* direction, so it is likely not analogous to peak C in the nickel complex. This peak may in fact be due to state transitions analogous to transitions $1 \rightarrow 12$ and $1 \rightarrow 13$ which are polarized close to perpendicular to *c* and are significantly to the red from the other transitions comprising peak G, but which are also derived from components of the $A_{1g} \rightarrow E_u$ transition in the single $Pt(CN)_4^{2-}$ ion.

Conclusions. We have found $Cs_2[Ni(CN)_4]\cdot H_2O$ to have a similar structure to $Cs_2[Pt(CN)_4]\cdot H_2O$ and the UV absorption spectra of the two complexes to be significantly red-shifted from solution. We have additionally calculated molecular orbitals and absorbance spectra for a limited segment of the $Cs_2[Ni(CN)_4]\cdot H_2O$ structure and have found that linear combination of molecular orbitals is sufficient to explain the spectral red shift upon crystallization in this class of complexes. It is also important to note that comparison of single-molecule transitions with those in the solid state must take into account the several state transitions resulting from the aggregation, as well as the fact, also present in the single molecule, that each state transition may be a composite of several orbital transitions.

Acknowledgment. The authors are grateful to Research Corporation and the National Science Foundation (Grant CHE9521548) for grants to R.L.M. We are also grateful to Ilana Pollack for her assistance in ZINDO calculations and to Dr. Yves Mantz for helpful discussions.

Supporting Information Available: Complete crystallographic data in CIF format, effective transitions for the Kramers−Kronig transformations, listings of all 123 molecular orbitals from ZINDO, and components of state transitions. Color depictions of thermal ellipsoids, an axial view of $Cs_2[Ni(CN)_4]\cdot H_2O$ crystal, coordination polyhedra for Cs, and orbitals 48−93. This material is available free of charge via the Internet at http://pubs.acs.org.

IC026101A

(44) Gray, H. B.; Ballhausen, C. J. *J. Am. Chem. Soc.* **1963**, *85*, 260.